ORIGINAL ARTICLE

Rod-like architecture and cross-sectional structure of an amyloid protofilament-like peptide supermolecule in aqueous solution

Takuma Minami[1,2], Sakiko Matsumoto[1,2], Yusuke Sanada[1,2], Tomonori Waku[3], Naoki Tanaka[3] and Kazuo Sakurai[1,2]

Synchrotron X-ray scattering was performed on an aqueous solution containing self-assembled aggregates of a β-sheet-forming peptide conjugated with a water-soluble moiety (polyethylene glycol, PEG or an oligo-peptide comprising a transactivator of transcription, TAT, sequence). The angular dependence of the scattering intensity in the low-q region (that is, $q < 2.0\,nm^{-1}$, where q is the magnitude of the scattering vector) indicated that the scattering objects were rod-like and completely dispersed in water without undergoing secondary aggregation. From the scattering intensity in the range of $0.5\,nm^{-1} < q < 5.0\,nm^{-1}$, it was deduced that the cross-section of the scattering objects was rectangular and not circular, presumably because of the laminated structure of the β-sheets. In the wide-angle region (that is, $q < 5.0\,nm^{-1}$), a diffraction peak was observed at $q = 13.4\,nm^{-1}$, which could be assigned to the two neighboring α-carbons of the peptide chains of the cross-section of the β-sheet. The scattering data indicated that the β-sheet-forming peptide indeed formed stacked β-sheets in a manner similar to that observed in the case of amyloid protofilaments, and that the resultant rod-like objects could be completely dispersed in water as a result of the hydrophilic PEG or TAT moiety.

INTRODUCTION

Amyloid fibrils are rod-like, highly protease-resistant protein aggregates that are found in the extracellular regions of organs and tissues. Previously, it was thought that amyloid fibrils do not have an active role in sustaining life but are instead a major cause of human diseases, including Alzheimer's and Parkinson's diseases.[1] Recently, the functional roles of amyloid fibrils have been elucidated, and thus, amyloid fibrils have attracted renewed attention.[2] In fact, amyloid fibrils have been found to possess other biological functions and can be used as antibacterial coatings or biofilms[3] and biological adhesives.[4] Amyloid-forming proteins do not exhibit sequence homologies close to one another but are rich in hydrophobic amino acids. When such proteins are assembled in the form of amyloid fibrils, the resultant fibers are typically unbranched, rigid rods with diameters of ~ 100 Å or greater. Amyloid fibrils are composed of several protofilaments with diameters of 20–35 Å.[1] In this sense, the protofilament is a substructure of the amyloid fibril and consists of highly ordered peptide chains that form a cross-β-structure in the fibrils. The term cross-β-structures refers to the β-sheets that are stacked on top of one another parallel to the fibril axis with their strands perpendicular to this axis.[5] Protofilaments are highly rigid and hydrophobic; therefore, it is quite difficult to disassemble amyloid fibrils into protofilaments and to prepare stable aqueous solutions in which protofilaments can be dispersed.[6]

With regard to supermolecular chemistry and nanomaterials, amyloid protofilaments and other rod-like peptide aggregates are attractive for use as building blocks, templates and biological scaffolds.[7–9] For instance, Stupp et al.[8] has studied a series of self-assembled rods made from peptide amphiphiles. One of the pioneering findings was a peptide-based scaffold that can be used as a biomaterial in tissue engineering. The excellent biocompatibility of peptides and the rod-like structure of entities suggest that these peptide-based rods have great potential for use in many novel therapies. Deechongkit et al.[10] synthesized a peptide-based, Π-shaped molecule comprising two peptide strands with β-sheet-forming sequences. The authors found that the Π-shaped molecules stacked to form a protofilament-like rod. The resultant rod seemed to be stabilized by the hydrophilic domains located on the outer layer of the rod. As a result, the very thin protofilament-like rods did not seem to form any secondary aggregates. To the best of our knowledge, their work was the first to observe an isolated and dispersed amyloid protofilament in water. Waku et al. synthesized several β-sheet-forming peptides that could be conjugated with both an antigen sequence and a water-soluble moiety (polyethylene glycol, PEG, or a transactivator of transcription, TAT, peptide sequence) with the aim of using these peptides for antigen delivery to immunocytes.[11–13] Their idea was to accelerate cellular ingestion by exploiting the strong

[1]Department of Chemistry and Biochemistry, The University of Kitakyushu, Fukuoka, Japan; [2]Structural Materials Science Laboratory SPring-8 Center, RIKEN Harima Institute Research, Hyogo, Japan and [3]Department of Biomolecular Engineering, Kyoto Institute of Technology, Kyoto, Japan
Correspondence: Professor K Sakurai, Department of Chemistry and Biochemistry, The University of Kitakyushu, 1-1 Hibikino, Wakamatsu-ku, Kitakyushu, Fukuoka, Japan.
E-mail: sakurai@kitakyu-u.ac.jp

characteristic of antigen-presenting cells to take up rods or other substrates with shapes that are rarely found in nature. Although they used β-sheet-forming peptides β-OVA-TAT, where β and OVA mean β-sheet and an ovalbumin peptide, respectively, and could observe the rod-like architecture with a length of ~240 nm using atomic force microscopy (see Figure 1), they could not obtain clear evidence that the β-sheet-forming peptides indeed formed protofilaments similar to those observed in amyloid fibrils.[11]

There are several critical requirements for identifying whether protofilaments are formed in a peptide or protein aggregate. Circular dichroism (CD) yields a characteristic band for β-sheets; however, it does not necessarily indicate the formation of cross-β-structures. To confirm the formation of these structures, the ordered β-sheet stacking, which exhibits two characteristic X-ray diffraction peaks corresponding to the β-sheet and β-strand distances ($d_1 = 1.15$ nm and $d_2 = 0.48$ nm, respectively), must be observed.[1,14] In particular, the presence of the peak at 0.48 nm is essential for confirming the presence of β-sheet stacking. Hamley and Krysmann[15] synthesized a PEG-conjugated, β-sheet-forming peptide and examined the competition between the PEG crystallization process and the fibrillization process attributed to the formation of the cross-β amyloid structure. They observed that fibrils dispersed in solutions exhibited diffractions related to the distance $d_2(= 0.48$ nm) corresponding to the cross-β-structures, indicating that the presence of the PEG chains did not disturb the cross-β-structures. To the best of our knowledge, there are few studies that have examined the overall conformation as well as the local structures of the aggregates of β-sheet-forming peptides. Avdeev *et al.*[16] performed neutron-scattering measurements on protein-oriented protofilaments in solution and analyzed the data using a helical rod model. In this study, we performed small-angle X-ray scattering (SAXS) measurements on aqueous solutions containing aggregates of β-sheet-forming peptides conjugated with both an antigen sequence and a water-soluble moiety studied by Waku *et al.*[11]

EXPERIMENTAL PROCEDURE

Materials and fibril formation
We prepared two peptide samples that contained a β-sheet-forming sequence, a model antigen (an OVA peptide) and hydrophilic chains of either ethylene
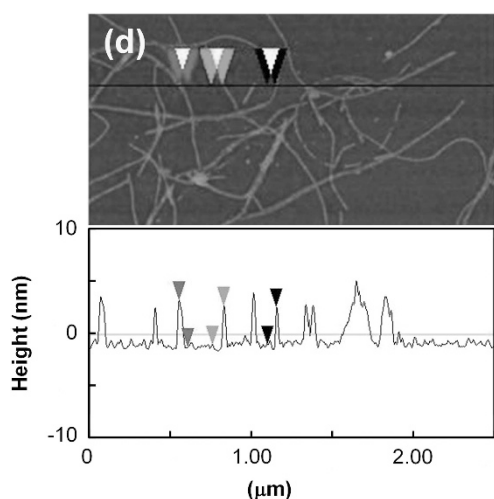
Figure 1 Typical AFM image and height profile of an aggregate formed by β-OVA-TAT (the chemical structure and the molecular weights are shown in Table 1), as reported in a previous work.[11] AFM, atomic force microscopy; OVA, ovalbumin; TAT, transactivator of transcription. A full color version of this figure is available at *Polymer Journal* online.

glycol or the TAT peptide chain (Figure 1). The sequences of these moieties are shown in the illustration below Table 1. We added a flexible space between the β-sheet sequence and the antigen to provide spatial freedom for both. β-OVA-TAT was purchased from Genscript (Piscataway, NJ, USA) and β-OVA-EG₁₂ was synthesized using a previously described method.[11] The samples were dissolved in a Dulbecco phosphate buffer solution, which was maintained at 60 °C for 24 h to allow the fibrils to form, as described in a previous paper.[11]

Circular dichroism measurements
The CD measurements were performed with a J-820 spectropolarimeter (JASCO, Tokyo, Japan). The samples were packed in 0.1 mm round quartz cells equipped with a water jacket to control the sample temperature, which was kept at 25 °C. The scanning wavelengths were 190–300 nm and the molecular ellipticity (θ) was calculated without taking into account the PEG weight.

Infrared absorption spectroscopy
The attenuated total reflection (ATR) infrared spectra of the nanofibers were obtained with a Spectrum One Fourier Transform-Infrared spectrometer (Perkin-Elmer, Waltham, MA, USA). The interferograms were co-added 16 times and Fourier-transformed at a resolution of 4 cm⁻¹.

X-ray scattering measurements
All the SAXS and wide-angle X-ray scattering (WAXS) measurements were performed at beam line 40B2 of the SPring-8 facility (Sayo, Hyogo, Japan). The sample solution was loaded in a quartz capillary cell (Hilgenberg GmbH, Malsfeld, Germany). The cell was then mechanically sealed with a silicone rubber gasket and placed in a vacuum chamber.[17] The X-ray wavelength (λ) and the sample-to-detector distance were 0.10 nm and 4.25 m, 0.10 nm and 1.82 m or 0.071 nm and 0.75 m, respectively. The first setup covered the range of 0.02 nm⁻¹ $< q <$ 2.03 nm⁻¹, the second setup covered the range of 0.05 nm⁻¹ $< q <$ 4.78 nm⁻¹ and the final setup covered the range of 0.18 nm⁻¹ $< q <$ 15.5 nm⁻¹. The scattered X-rays were detected with a 30 cm × 30- cm imaging plate (Rigaku, Tokyo, Japan, R-AXIS VII). After subtracting the solvent scattering from the solution scattering, we obtained the scattering only from the solute molecules. The concentrations of the β-OVA-EG₁₂ and β-OVA-TAT samples were 5.1 and 5.4 mg ml⁻¹, respectively. We confirmed that the particle interference was negligibly small at these concentrations.

Calculating the scattering intensity for rod-like objects
The scattering intensity, $I(q)$, is related to the pair-correlation function, $p(r)$, for the scattering objects through the Fourier transform:[18,19]

$$I(\vec{q}) = \int_V p(\vec{r}) \exp(-i\,\vec{r}\cdot\vec{q})\,d\vec{r} \tag{1}$$

where $\vec{q}$ is the scattering vector. When the scattering objects are infinitely long along one direction (assuming the z-direction in this case) and randomly

Table 1 Molecular designs, chemical structures and molecular weights of the β-sheet-forming peptide conjugated with a hydrophilic chain and OVA antigen

	β-sheet	*Spacer*	*Antigen*	*Hydrophilic part*
β-OVA-EG₁₂	FVIFLD	GSG	SIINFEKL	(C₂H₄O)₁₂-H
	717.88	183.18	927.11	529.60
β-OVA-TAT	FVIFLD	GSG	SIINFEKL	RKKRRQRRR
	717.88	183.18	927.11	1320.59

N   β sheet part   Antigen part   Hydrophilic part   C

Abbreviations: OVA, ovalbumin; TAT, transactivator of transcription. A full color version of this figure is available at *Polymer Journal* online.
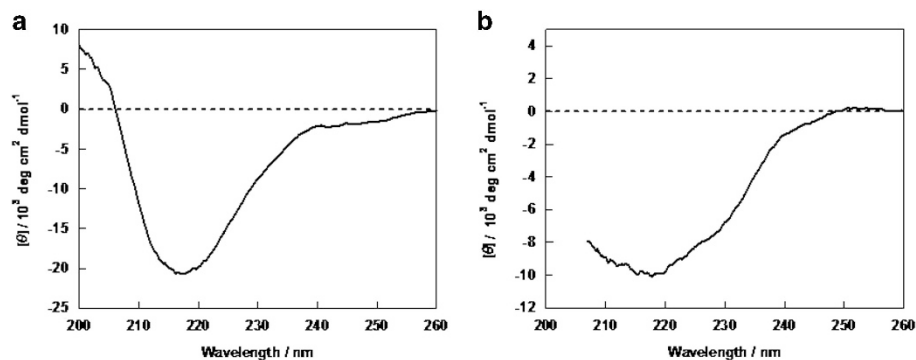
Figure 2 CD spectra of (a) β-OVA-EG12 and (b) β-OVA-TAT. CD, circular dichroism; OVA, ovalbumin; TAT, transactivator of transcription.

oriented in the solution, this relation can be reduced to the following equation:[17,18]

$$I(q) \propto \frac{1}{q} \int_S p_{2D}(r) J_0(rq) \mathrm{d}r \qquad (2)$$

where $p_{2D}(r)$ is the correlation function for the x-y plain perpendicular to the rod axis (z). We assume that the electron-density distribution does not depend on z. Furthermore, J_0 is a zeroth-order Bessel function. In this paper, we use two models: solid cylinder and solid square pole, where the former has a circle cross-section and the latter has a square cross-section. Once the cross-sectional shape is given, $p_{2D}(r)$ can be analytically or numerically calculated and then the scattering intensity can be obtained as a function of q.

As is the case with the radius of gyration for the scattering from isolated particles, we can define a cross-sectional radius of gyration, (R_{cg}),[17,18] which can be determined from the following equation:

$$q I(q) \propto \exp\left(-\frac{1}{2}R_{cg}^2 q^2\right) \qquad (3)$$

RESULTS AND DISCUSSION

Circular dichroism

Figure 2 shows the CD spectra of β-OVA-EG12 and β-OVA-TAT. Both samples exhibited a minimum at 220 nm. According to previous studies,[20–22] this negative band at 220 nm indicates the presence of β-sheets. β-OVA-TAT showed an additional negative band at ~ 200 nm, which was presumably ascribed to the random coil-like conformation of the TAT moiety. Upon comparing the two samples, we found that β-OVA-EG12 showed a stronger negative band at 220 nm than did β-OVA-TAT. This observation is likely attributed to the fact that the β-sheets are stacked to a greater degree in β-OVA-EG12 than in β-OVA-TAT or that β-OVA-EG12 simply contains more β-sheets than β-OVA-TAT. This result may be interpreted to mean that the TAT moieties conjugated to the β-sheet-forming portion interfere in the formation and stacking of the β-sheets.

The difference in the two samples was in the chemical structure of the hydrophilic moieties, which were EG12 and TAT. TAT is considered a water-compatible chain and thus has a random coil-like conformation, which yields a characteristic CD signal.[23] However, the fact that TAT exhibits CD indicates that it is ordered to some extent. In fact, the random coil-like conformations of peptides are not completely random but rather can be considered a fluctuating peptide helix that is conformationally similar to the left-handed polyproline II helix.[24] However, the EG12 chain does have a random coil-like conformation. We assumed that the presence of ordering in the TAT chain is the reason that the degree of stacking of β-sheets in β-OVA-TAT was low.
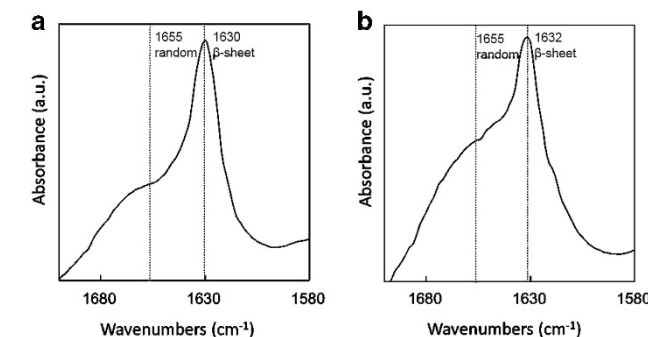

Figure 3 IR spectra of (a) β-OVA-EG12 and (b) β-OVA-TAT. IR, infrared; OVA, ovalbumin; TAT, transactivator of transcription.

Infrared absorption spectroscopy

Figure 3 compares the IR spectra of β-OVA-EG$_{12}$ and β-OVA-TAT. According to previous studies,[23] peptide β-sheets exhibit a characteristic peak at 1632 cm^{-1} in their IR absorption spectra. This sheet can be ascribed to the amide I band, which is primarily related to the stretching vibrations of the main-chain carbonyl groups of the peptides. The intensity and position of the amide I band yield direct structural information regarding the polypeptide backbone and its secondary structures. As shown in Figure 3, both β-OVA-EG$_{12}$ and β-OVA-TAT show this characteristic amide I peak, confirming the presence of β-sheets. Upon comparing the amide I peaks on the two samples, we found that β-OVA-EG$_{12}$ showed a higher intensity peak than β-OVA-TAT, indicating that β-OVA-EG$_{12}$ contains a greater number of β-sheets. In addition, the IR absorption observed for 1630–1680 cm^{-1} could be ascribed to the disordered structures of the peptide backbone. As seen in the figure, β-OVA-TAT has a greater number of disordered peptide chains than β-OVA-EG$_{12}$. These structural characteristics determined from the IR spectra are consistent with those determined from the CD measurements.

Synchrotron small-angle X-ray scattering

Figure 4a shows the scattering profiles of the two samples in the range of 0.05 nm^{-1} < q < 5.00 nm^{-1}. The profiles were obtained by combining the three sets of data obtained from the three setups. For q < 0.3 nm^{-1}, the scattering intensity, $I(q)$, satisfies the relation $I(q) \propto q^{-1}$, as is expected for infinitely long thin rods.[19] This relation indicates that both samples had a rod-like architecture and did not exhibit branching. With an increase in q beyond this range, $I(q)$ deviated from the limit characteristic of rods because of the finite cross-sectional area. On the basis of this deviation, we calculated the cross-sectional radius of gyration (R_{cg}) using Equation 3. Panel b
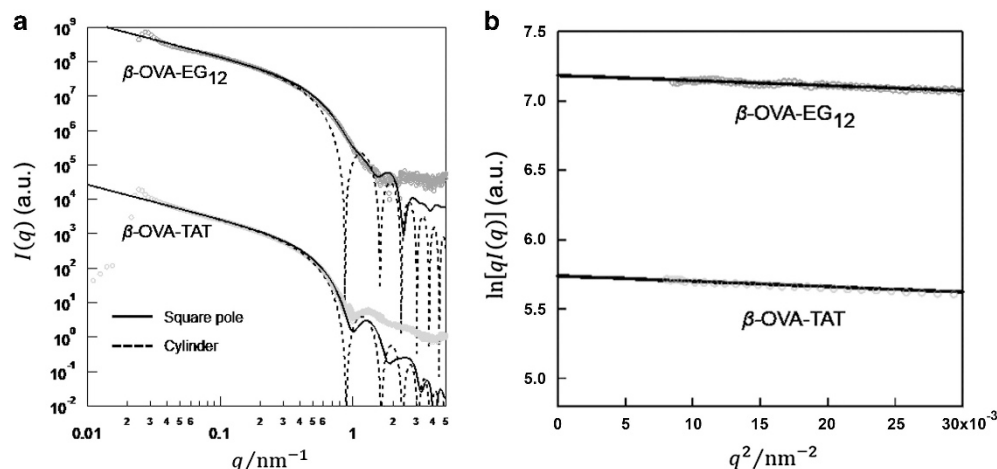
Figure 4 (**a**) SAXS profiles of β-OVA-EG$_{12}$ (red) and β-OVA-TAT (green). The cylinder and rectangular modes resulted in the same R_{cg} values, which are compared with those obtained from the cross-sectional Guinier plot. The data points for β-OVA-EG$_{12}$ were vertically shifted by multiplying them by 104.3 for comparison. (**b**) Cross-sectional Guinier plots for β-OVA-EG$_{12}$ (red) and β-OVA-TAT (green). OVA, ovalbumin; SAXS, small-angle X-ray scattering; TAT, transactivator of transcription. A full color version of this figure is available at *Polymer Journal* online.

shows the plots of $\ln[qI(q)]$ versus q^2 for the two samples; the R_{cg} values were determined from the slopes of the plots. The resultant values, which are listed in the second column in Table 2, were very similar.

Although the R_{cg} values were similar, the degrees of scattering for high-q values were quite different. β-OVA-TAT showed a maximum at approximately $q = 1.3$ nm^{-1}, which can be ascribed to the form factor for the cross-sectional density distribution. However, β-OVA-EG$_{12}$ did not show such a maximum. The presence of the second maximum corresponding to the form factor can be explained by any of the following factors: β-OVA-TAT has a more uniform structure along the axis than does β-OVA-EG$_{12}$, β-OVA-TAT has a more ordered cross-sectional structure than does β-OVA-EG$_{12}$, or the Gaussian-chain scattering attributed to the PEG moieties overwhelms the other scatterings in the high-q region. At this moment, we do not have enough data to state the primary reason for the difference in the high-q scatterings.

When the electron density in the x-y plane is constant and the cross-section is circular, the so-called solid cylinder model with a cylinder radius of $R_{s\text{-cylinder}}$ is adopted, where $R_{s\text{-cylinder}}$ is related to R_{cg} by

$$R_{cg} = \sqrt{\frac{1}{2}} R_{s-cylinder} \qquad (4)$$

The dotted lines in Figure 4a represent the scattering profiles calculated using the solid cylinder model and the $R_{s\text{-cylinder}}$ values calculated from R_{cg} using Equation 4. Upon comparing these calculated curves with the experimental data, it can be seen that the solid cylinder model closely represents the data for q-values of up to ~0.6 nm^{-1} for β-OVA-EG$_{12}$ and ~0.7 nm^{-1} for β-OVA-TAT; however, the calculated and experimental data deviate with an increase in q. In the case of β-OVA-EG$_{12}$, a second intensity maximum was not observed experimentally; however, the model indicated a maximum at ~1.3 nm^{-1}. For β-OVA-TAT, both the experimental data and the model suggested a second maximum; however, the positions were different in that the model indicated that the maximum occurred at a smaller q-value than that suggested by the experimental data. These discrepancies indicate that a more elaborate model might be required to fit the data.

Table 2 Obtained parameters of the β-OVA-EG12 and β-OVA-TAT

Sample code	R_{cg}/nm	$L_1 \times L_2$/nm × nm	
		SAXS	AFM
β-OVA-EG$_{12}$	2.72 ± 0.10	8.0 × 5.0	4.6 ± 0.4 × 3.7 ± 0.3
β-OVA-TAT	2.79 ± 0.05	7.5 × 6.1	4.6 ± 0.5 × 3.8 ± 0.3

Abbreviations: AFM, atomic force microscopy; OVA, ovalbumin; SAXS, small-angle X-ray scattering; TAT, transactivator of transcription.

Wide-angle X-ray scattering

Figure 5 shows the WAXS profiles of the two samples. Both samples exhibited a significant diffraction peak at $q = 13.4$ nm^{-1}, and β-OVA-TAT also showed a small peak at $q = 5.5$ nm^{-1}. The distance for the peak at $q = 13.4$ nm^{-1}, calculated from the Bragg equation, was 0.47 nm. This peak could be assigned to the lattice diffraction between the two neighboring α-carbons of the peptide chains of the cross-β-sheet, as depicted in Figure 5b.[1,14] The presence of this peak was a clear indication that the rod-like aggregates of β-OVA-EG12 and β-OVA-TAT consisted of stacked β-sheets. In other words, the rod-like objects of β-OVA-EG12 and β-OVA-TAT were identified as having a structure similar to that of protofilaments. The peak at $q = 5.5$ nm^{-1} could be assigned to the diffraction from the two adjacent peptide chains within the β-sheet, as shown in Figure 5b.

Using a square pole model to fit the SAXS data

The SAXS analysis indicated that β-OVA-EG$_{12}$ and β-OVA-TAT possessed rod-like structures. As mentioned above, we made an attempt to fit the data using a cylinder model with the same R_{cg} values as those of the samples; however, the high-q scatterings could not be fitted using this model. The fact that CD occurred indicated the presence of β-sheets. The WAXS analysis suggested that stacked β-sheets formed the β-OVA-EG$_{12}$ and β-OVA-TAT rods. According to previous XRD studies,[1,14] in the characteristic cross-β-structure, the β-strands are arranged perpendicular to the fibril axis and the ribbon-like β-sheets are parallel to the fibril axis. Thus, it was reasonable to assume that the β-sheet-forming sequence in the synthesized samples was arranged in the same manner. If this is
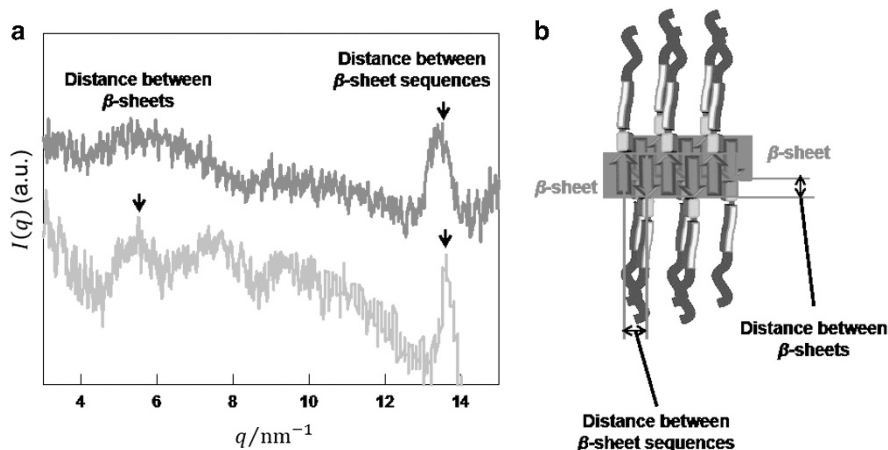
Figure 5 (**a**) WAXS profiles of β-OVA-EG12 (red, upper line) and β-OVA-TAT (green, lower line). (**b**) A schematic showing β-sheet packing. OVA, ovalbumin; TAT, transactivator of transcription; WAXS, wide-angle X-ray scattering. A full color version of this figure is available at *Polymer Journal* online.
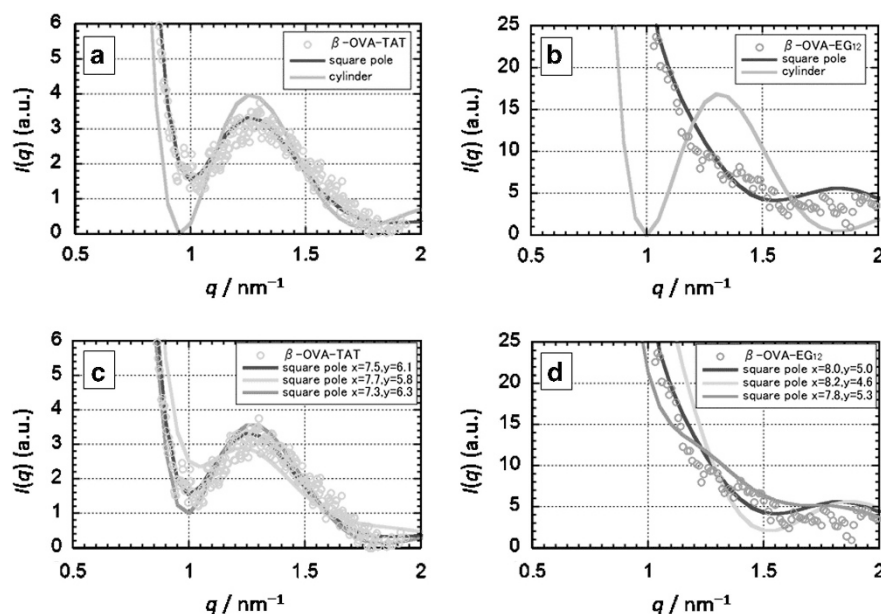

Figure 6 Comparison of the experimental SAXS data and the fits made using the square pole and cylinder models. SAXS, small-angle X-ray scattering. A full color version of this figure is available at *Polymer Journal* online.
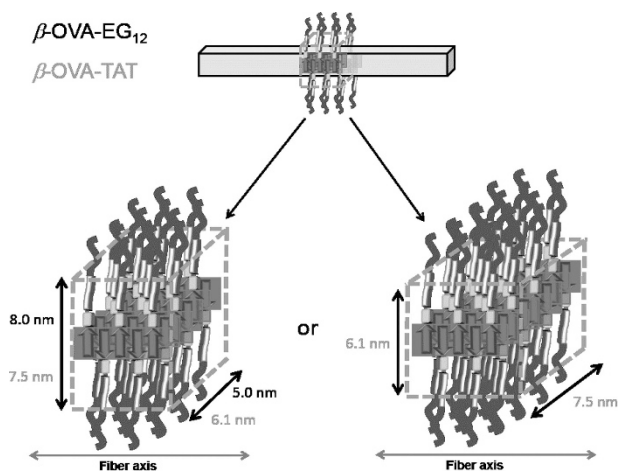

Figure 7 Schematic of the local structures of β-OVA-EG12 and β-OVA-TAT. OVA, ovalbumin; TAT, transactivator of transcription. A full color version of this figure is available at *Polymer Journal* online.

indeed the case, the cross-section of the rod must be rectangular, that is, the data should be such that they can be fitted using a square pole rather than a cylinder. It can be assumed that the helix model used by Avdeev[16] might be better than the square pole model. However, we did not observe any helical patterns in either the atomic force microscopy or the transmission electron microscopy images;[11] therefore, we did not use such a model.

We attempted to fit the data with a square pole model having the same R_{cg} values as the samples by changing the ratio of the two sides of the rectangle, where R_{cg} is related to the lengths of the two sides (L_1 and L_2) through the following equation:[19]

$$R_{cg} = \sqrt{\frac{1}{3}\left(\frac{L_1^2}{4} + \frac{L_2^2}{4}\right)} \qquad (6)$$

The blue lines in Figures 6a and b indicate the best model for each sample. The side lengths are listed in Table 2, which were 8.0 nm × 5.0 nm for β-OVA-EG12 and 7.5 nm × 6.1 nm for β-OVA-TAT.

Figures 6c and d compare the curves obtained for different sets of the side lengths, indicating that the best-fitting lengths were determined with an error margin of ± 0.4 nm (light blue and purple lines). The square pole models with the best parameters were compared with the data for the entire range (solid lines). As shown in Figures 4 and 6, the square pole model could reproduce the data with greater fidelity than the cylinder model. As seen in Figure 1, the atomic force microscopy and transmission electron microscopy images obtained by Waku *et al.* indicate that the aggregates exhibit two distinct heights (see Supplementary Figure SI.1 of Supplementary Information). The fact that there are two heights is consistent with the square pole model, even though the absolute values were slightly different because of the experimental error.

The high-q SAXS profiles could be fitted well using a square pole model, that is, using the values 8.0×5.0 nm for β-OVA-EG12 and 7.5×6.0 nm for β-OVA-TAT; however, the WAXS patterns indicated β-sheet stacking. The occurrence of CD and IR indicated that β-OVA-EG12 contains a greater number of β-sheets than does β-OVA-TAT. On the basis of these experimental results, the most likely arrangements for β-OVA-EG12 can be assumed, which are shown in Figure 7. Given that the number of β-sheets in β-OVA-EG12 was higher than in β-OVA-TAT, the side length of 8.0 nm may correspond to the size of the β-sheets with the thickness of the stack being 5.0 nm. The length of the complete β-sheet-forming peptide is ~ 2.28 nm; therefore, some of the OVA antigen sequences may be involved in the formation of the sheets. In the case of β-OVA-TAT, the two side lengths are too similar in value to allow one to say which one might be the width of the β-sheets. For both samples, neither TAT nor PEG is involved in rod formation. Furthermore, they are presumably oriented randomly around the pole such that they can interact favorably with water molecules. The presence of these hydrophilic chains prevents the protofilament-like rods from undergoing secondary aggregation.

CONCLUSIONS

To conclude, we found that the angular dependence of the scattering intensity in the low-q region indicates that the scattering objects could be described using a square pole model. Furthermore, the objects could completely disperse in water. For the range of 0.5 nm$^{-1} < q < 5.0$ nm^{-1}, the cross-section of the scattering objects was rectangular and not circular, presumably related to the laminated structure of the β-sheets. In the wide-angle region, a diffraction peak was observed at $q = 13.4$ nm^{-1} as a result of the two neighboring α-carbons of the peptide chains of the cross-β-sheet. The scattering data indicated that the β-sheet-forming peptide indeed formed stacked β-sheets in a manner nearly identical to that of amyloid protofilaments.

CONFLICT OF INTEREST

The authors declare no conflict of interest.

1 Jiménez, J. L., Nettleton, E. J., Bouchard, M., Robinson, C. V., Dobson, C. M. & Saibil, H. R. The protofilament structure of insulin amyloid fibrils. *Proc. Natl Acad. Sci. USA* **99**, 9196–9201 (2002).
2 Knowles, T. P. & Buehler, M. J. Nanomechanics of functional and pathological amyloid materials. *Nat. Nanotechnol.* **6**, 469–479 (2011).
3 Maji, S. K., Perrin, M. H., Sawaya, M. R., Jessberger, S., Vadodaria, K., Rissman, R. A., Singru, P. S., Nilsson, K. P. R., Simon, R. & Schubert, D. Functional amyloids as natural storage of peptide hormones in pituitary secretory granules. *Science* **325**, 328–332 (2009).
4 Mostaert, A. S., Higgins, M. J., Fukuma, T., Rindi, F. & Jarvis, S. P. Nanoscale mechanical characterisation of amyloid fibrils discovered in a natural adhesive. *J. Biol. Phys.* **32**, 393–401 (2006).
5 Nelson, R., Sawaya, M. R., Balbirnie, M., Madsen, A. O., Riekel, C., Grothe, R. & Eisenberg, D. Structure of the cross-[beta] spine of amyloid-like fibrils. *Nature* **435**, 773–778 (2005).
6 Chiti, F., Bucciantini, M., Capanni, C., Taddei, N., Dobson, C. M. & Stefani, M. Solution conditions can promote formation of either amyloid protofilaments or mature fibrils from the HypF N-terminal domain. *Protein Sci.* **10**, 2541–2547 (2001).
7 Colombo, G., Soto, P. & Gazit, E. Peptide self-assembly at the nanoscale: a challenging target for computational and experimental biotechnology. *Trends Biotechnol.* **25**, 211–218 (2007).
8 Cui, H., Cheetham, A. G., Pashuck, E. T. & Stupp, S. I. Amino acid sequence in constitutionally isomeric tetrapeptide amphiphiles dictates architecture of one-dimensional nanostructures. *J. Am. Chem. Soc.* **136**, 12461–12468 (2014).
9 Pashuck, E. T., Cui, H. & Stupp, S. I. Tuning supramolecular rigidity of peptide fibers through molecular structure. *J. Am. Chem. Soc.* **132**, 6041–6046 (2010).
10 Deechongkit, S., Powers, E. T., You, S.-L. & Kelly, J. W. Controlling the morphology of cross β-sheet assemblies by rational design. *J. Am. Chem. Soc.* **127**, 8562–8570 (2005).
11 Waku, T., Kitagawa, Y., Kawabata, K., Nishigaki, S., Kunugi, S. & Tanaka, N. Self-assembled β-sheet peptide nanofibers for efficient antigen delivery. *Chem. Lett.* **42**, 1441–1443 (2013).
12 Fukuhara, S., Nishigaki, T., Miyata, K., Tsuchiya, N., Waku, T. & Tanaka, N. Mechanism of the chaperone-like and antichaperone activities of amyloid fibrils of peptides from αA-crystallin. *Biochemistry* **51**, 5394–5401 (2012).
13 Tanaka, N., Tanaka, R., Tokuhara, M., Kunugi, S., Lee, Y.-F. & Hamada, D. Amyloid fibril formation and chaperone-like activity of peptides from αA-crystallin. *Biochemistry* **47**, 2961–2967 (2008).
14 Sunde, M., Serpell, L. C., Bartlam, M., Fraser, P. E., Pepys, M. B. & Blake, C. C. Common core structure of amyloid fibrils by synchrotron X-ray diffraction. *J. Mol. Biol.* **273**, 729–739 (1997).
15 Hamley, I. W. & Krysmann, M. J. Effect of PEG crystallization on the self-assembly of PEG/peptide copolymers containing amyloid peptide fragments. *Langmuir* **24**, 8210–8214 (2008).
16 Avdeev, M. V., Aksenov, V. L., Gazová, Z., Almásy, L., Petrenko, V. I., Gojzewski, H., Feoktystov, A. V., Siposova, K., Antosova, A., Timko, M. & Kopcansky, P. On the determination of the helical structure parameters of amyloid protofilaments by small-angle neutron scattering and atomic force microscopy. *J. Appl. Crystallogr.* **46**, 224–233 (2013).
17 Akiba, I., Terada, N., Hashida, S., Sakurai, K., Sato, T., Shiraishi, K., Yokoyama, M., Masunaga, H., Ogawa, H., Ito, K. & Yagi, N. Encapsulation of a hydrophobic drug into a polymer-micelle core explored with synchrotron SAXS. *Langmuir* **26**, 7544–7551 (2010).
18 Roe, R.-J. *Methods of X-ray and Neutron Scattering in Polymer Science* (Oxford Univ. Press on Demand, 2000).
19 Glatter, O. & Kratky, O. *Small Angle X-ray Scattering* (Academic, 1982).
20 Smith, K. F., Harrison, R. A. & Perkins, S. J. Molecular modeling of the domain structure of C9 of human complement by neutron and x-ray solution scattering. *Biochemistry* **31**, 754–764 (1992).
21 Lashuel, H. A., LaBrenz, S. R., Woo, L., Serpell, L. C. & Kelly, J. W. Protofilaments, filaments, ribbons, and fibrils from peptidomimetic self-assembly: implications for amyloid fibril formation and materials science. *J. Am. Chem. Soc.* **122**, 5262–5277 (2000).
22 *Circular Dichroism: Principles and Applications*, 2nd edn (John Wiley & Sons Inc, 2000).
23 Dukor, R. K. & Keiderling, T. A. Reassessment of the random coil conformation: vibrational CD study of proline oligopeptides and related polypeptides. *Biopolymers* **31**, 1747–1761 (1991).
24 Hilderson, J. H. & Ralston, G. B. in *Subcellular Biochemistry*, Vol. 23 (eds Hilderson, J. H & Ralston, G. B.) (Plenum Press, New York, NY, USA, 1994).

Supplementary Information accompanies the paper on Polymer Journal website (http://www.nature.com/pj)